

Correlation of the Apparent Diffusion Coefficient (ADC) with the Standardized Uptake Value (SUV) in Hybrid 18F-FDG PET/MRI in Non-Small Cell Lung Cancer (NSCLC) Lesions: Initial Results

Korrelation des scheinbaren Diffusionskoeffizienten (ADC) mit dem „standardized uptake values“ (SUV) bei nichtkleinzelligen Bronchialkarzinomen (NSCLC) in einem hybriden 18F-FDG-PET/MR

Authors

P. Heusch¹, C. Buchbender¹, J. Köhler², F. Nensa³, K. Beiderwellen³, H. Kühl³, R. S. Lanzman¹, H. J. Wittsack¹, B. Gomez⁴, T. Gauler², M. Schuler², M. Forsting³, A. Bockisch⁴, G. Antoch¹, T. A. Heusner¹

Affiliations

Affiliation addresses are listed at the end of the article.

Key words

- thorax
- MR diffusion/perfusion
- PET-CT

Zusammenfassung

Ziel: Vergleich der in der kombinierten 18F-FDG-PET/MR bzw. 18F-FDG-PET/CT ermittelten, scheinbaren Diffusionskoeffizienten (ADC) und der „standardized uptake values“ (SUV) bei nichtkleinzelligen Bronchialkarzinomen (NSCLC).

Material und Methoden: Bei 18 konsekutiven Patienten mit histologisch gesichertem NSCLC (17 Männer, 1 Frau, mittleres Alter: 61 ± 12 Jahre) wurde nach einer Ganzkörper-FDG-PET/CT eine Ganzkörper-FDG-PET/MR durchgeführt. Um den maximalen und mittleren SUV (SUV_{max} ; SUV_{mean}) zu bestimmen, wurden die Grenzen des Primärtumors identifiziert und ein „volume of interest“ (VOI) in der FDG-PET/CT und FDG-PET/MR platziert. Eine „region of interest“ (ROI) wurde manuell, den ganzen Tumor umfassend, in die Bilder der diffusionsgewichteten Sequenzen ($b=0$) eingezeichnet und anschließend in die Parameterkarten transferiert, um die ADC-Werte zu ermitteln. Um die SUV- und ADC-Werte zu vergleichen, wurde der Pearson Korrelationskoeffizient gebildet.

Ergebnisse: Der SUV_{max} der NSCLC betrug $12,3 \pm 4,8$ [Mittelwert ± Standardabweichung], der SUV_{mean} betrug $7,2 \pm 2,8$, gemessen in der FDG-PET/MR. Die mit Hilfe der FDG-PET/CT und FDG-PET/MR gemessenen SUV_{max} - und SUV_{mean} -Werte korrelierten jeweils sehr gut ($R=0,93$; $p<0,001$ und $R=0,92$; $p<0,001$). Der mittlere ADC (ADC_{mean}) der Lungentumore war $187,9 \pm 88,8 \times 10^{-5} \text{ mm}^2/\text{s}$ [Mittelwert ± Standardabweichung]. Der mit Hilfe der FDG-PET/MR gemessene ADC_{mean} wies eine signifikante, inverse Korrelation mit dem SUV_{max} ($R=-0,72$; $p<0,001$) als auch mit dem SUV_{mean} ($R=-0,71$; $p<0,001$) auf.

Schlussfolgerung: Es besteht sowohl eine exzellente Korrelation zwischen dem SUV_{max} und SUV_{mean} , ermittelt in der FDG-PET/CT und der darauf folgenden FDG-PET/MR, als auch eine signifikante, inverse Korrelation zwischen dem

Abstract

Purpose: To compare the apparent diffusion coefficient (ADC) in non-small cell lung cancer lesions with standardized uptake values (SUV) derived from combined 18F-fluoro-deoxy-glucose-positron emission tomography/magnetic resonance imaging (FDG-PET/MRI) and those derived from FDG-PET/CT.

Materials and Methods: In 18 consecutive patients with histologically proven NSCLC (17 men, 1 woman; mean age, 61 ± 12 years), whole-body FDG-PET/MRI was performed after whole-body FDG-PET/CT. Regions of interest (ROI) encompassing the entire primary tumor were drawn into FDG-PET/CT and FDG-PET/MR images to determine the maximum and mean standardized uptake value (SUV_{max} ; SUV_{mean}) and into ADC parameter maps to assess mean ADC values. Pearson's correlation coefficients were calculated to compare SUV and ADC values.

Results: The SUV_{max} of NSCLC was 12.3 ± 4.8 [mean ± SD], and the SUV_{mean} was 7.2 ± 2.8 as assessed by FDG-PET/MRI. The SUV_{max} and SUV_{mean} derived from FDG-PET/CT and FDG-PET/MRI correlated well ($R=0.93$; $p<0.001$ and $R=0.92$; $p<0.001$, respectively). The ADCmean of the pulmonary tumors was $187.9 \pm 88.8 \times 10^{-5} \text{ mm}^2/\text{s}$ [mean ± SD]. The ADC_{mean} exhibited a significant inverse correlation with the SUV_{max} ($R=-0.72$; $p<0.001$) as well as with the SUV_{mean} assessed by FDG-PET/MRI ($R=-0.71$; $p<0.001$).

Conclusion: This simultaneous PET/MRI study corroborates the assumed significant inverse correlation between increased metabolic activity on FDG-PET and restricted diffusion on DWI in NSCLC.

Citation Format:

► Heusch P, Buchbender C, Köhler J et al. Correlation of the Apparent Diffusion Coefficient (ADC) with the Standardized Uptake Value (SUV) in Hybrid 18F-FDG PET/MRI in Non-

eingereicht 31.12.2012
akzeptiert 2.6.2013

Bibliography

DOI <http://dx.doi.org/10.1055/s-0033-1350110>
Published online: 16.7.2013
Fortschr Röntgenstr 2013; 185: 1056–1062 © Georg Thieme Verlag KG Stuttgart · New York · ISSN 1438-9029

Correspondence

Dr. Christian Buchbender
Department of Diagnostic and Interventional Radiology, D-40225 Dusseldorf, Germany, Univ Dusseldorf, Medical Faculty Moorenstr. 5 40225 Dusseldorf Germany
Tel.: ++49/2 11/8 11 77 52
Fax: ++49/2 11/8 11 61 45
christian.buchbender@med.uni-duesseldorf.de

SUV_{max}, dem SUV_{mean} und dem ADC_{mean}, ermittelt mit Hilfe der FDG-PET/MR.

Small Cell Lung Cancer (NSCLC) Lesions: Initial Results. Fortschr Röntgenstr 2013; 185: 1056–1062

Introduction

Lung cancer is the most frequently diagnosed cancer with one of the highest cancer mortalities globally [1]. Non-small cell lung cancer (NSCLC) accounts for approximately 80% of all bronchogenic malignancies [1]. For a stage-adapted therapy and thus an individual therapeutic concept, ¹⁸F-fluoro-desoxy-glucose-positron emission tomography/computed tomography (FDG-PET/CT) is accepted as the diagnostic modality of choice, because of its high accuracy for the detection of the primary lesion and metastases in particular [2]. Furthermore, the maximum standard uptake value (SUV_{max}) of NSCLC assessed by FDG-PET/CT is established as an independent marker of tumor characteristics [3].

Apart from PET/CT, magnetic resonance imaging (MRI) offers great potential in the detection and interpretation of malignancies [4]. Especially diffusion-weighted MR imaging (DWI) is a sensitive tool for lesion detection (primary tumors, nodal and distant metastases) in various malignancies and yields comparable results to FDG-PET/CT in some tumor subtypes [5–7]. Due to the bright appearance of malignant lesions on high-b-value DWI images, which provide a high lesion-to-background ratio, DWI commonly serves as a “search-sequence” with a PET-like appearance. Therefore, DWI is included in whole-body MRI staging protocols in many centers. DWI may also increase the specificity when it comes to lesion interpretation by quantification of the apparent diffusion coefficient (ADC). In malignant lesions the increased cellular density restricts water diffusion in the interstitial space, resulting in lower ADC values than in inflammatory reactive tissue or scar tissue [8, 9]. In a previous study the potential of DWI in the differentiation of malignant from benign pulmonary lesions has been demonstrated [10]. Matoba et al. reported a significant correlation between ADC values and the degree of cell differentiation in patients with lung cancer [11].

Recently introduced whole-body integrated PET/MRI scanners enable truly simultaneous acquisition and highly accurate spatial co-registration of PET and MRI data sets [12, 13]. Apart from and in addition to the lack of ionizing radiation as compared with CT, MRI in combination with PET is expected to provide a new quality in functional cancer imaging [14], mainly due to the combination of functional MR and PET information. Already published clinical studies using whole-body PET/MRI in oncologic patients confirmed its feasibility for whole-body cancer staging and reported an image quality comparable to that of PET/CT for lesion detection [15–17]. In a pilot study with 10 patients, Schwenzer et al. recently highlighted the potential of PET/MR for the assessment of pulmonary masses, showing a similar lesion characterization and tumor stage compared to PET/CT [16].

Regier and colleagues demonstrated a significant inverse correlation between the SUV_{max} determined by FDG-PET/CT and the ADC in NSCLC [18]. Recently, the use of ADC values derived from simultaneous DWI and PET acquisitions in a whole-body PET/MRI scanner has been proven to be stable for clinical applications [19]. The relation between SUV values and ADC values of NSCLCs when assessed by a simultaneous PET/MRI examination has not been examined yet.

Therefore, the aim of this study was to correlate the tracer uptake of NSCLC, as reflected by SUVs derived from FDG-PET/MRI using

MR attenuation correction with ADC values derived from simultaneous DWI MRI measurements.

Materials and Methods

Patients

In 18 consecutive patients with histologically proven NSCLC (17 men, 1 woman; age 61 ± 12 years), whole-body FDG-PET/MRI was performed (no additional ¹⁸F-FDG injection) after routine clinical FDG-PET/CT (60 min after injection of 300 ± 40 MBq ¹⁸F-FDG). All patient histories revealed no prior malignant disease and no chemotherapy or radiotherapy. Written informed consent was obtained from all participants. This study was performed in accordance with the regulations of the local institutional ethics committee.

PET/CT Imaging

Whole-body (WB) FDG-PET/CT scans were obtained on a mCTTM PET/CT scanner (Siemens Molecular Imaging, Hoffmann, Estates, IL, USA), containing 32.440 4 × 4 mm LSO crystals for PET imaging. Before imaging, patients fasted for at least 6 h. All patients had blood glucose levels below 150 mg/dL at the time of ¹⁸F-FDG injection. ¹⁸F-FDG (300 ± 40 MBq) was intravenously injected 60 min before the scan. The contrast-enhanced CT scan was taken with the following parameters: caudocranial scan direction, field of view: skull base to upper thighs, 120 kV, automatic mA/s adjustment (Care Dose 4DTM, preset: 210 mAs), 5 mm slice thickness, 5 mm increment, pitch 1. PET scan: 3D mode, 2 min emission time per bed position (45% overlap), reconstruction according to the ordered subsets expectation maximization (OSEM) algorithm with 4 iterations and 8 subsets, 3D Gaussian filter, 4.0 mm, full width at half maximum (FWHM), scatter correction. The attenuation correction was based on the portalvenous phase of whole-body CT.

PET/MR Imaging

WB FDG PET/MRI was performed on a Magnetom Biograph mMRTM (Siemens Healthcare, Erlangen, Germany), containing a total of 28.672 LSO crystals for PET-measurement. FDG-PET/MRI was performed following FDG-PET/CT with a mean delay of 80 ± 13 min. The field of view (FoV) contained the body volume from the head to the thighs. The PET acquisition time was 20 min for the entire thorax. PET images were reconstructed using the iterative algorithm OSEM, 3 iterations and 21 subsets, Gaussian filter: FWHM 4.0 mm; scatter correction. A dedicated mMR head and neck coil and, depending on the patients' height, up to 4 mMR body flex coils were used for MR imaging. MR imaging was performed simultaneously to PET imaging using the following sequence protocol for each bed position:

1. a coronal 3-dimensional volume interpolated gradient echo (VIBE) sequence (repetition time (TR) 3.6 ms, echo time 1 (TE1) 1.23 ms, TE2 2.46 ms, 3.12 mm slice thickness, FoV 500 mm for DIXON-based attenuation correction);
2. a coronal T2-weighted steady state free precession (TrueFISP) sequence of the thorax (TR 3.75 ms, TE 1.64 ms, matrix size

- 320, 6 mm slices, FoV 330 mm, generalized auto calibrating partially parallel acquisition (GRAPPA; acceleration factor 2);
3. a transverse T2-weighted blade turbo spin echo sequence of the thorax in breath-hold technique (TR 4360 ms, TE 160 ms, matrix size 384, 5 mm slices, FoV 400 mm, GRAPPA, acceleration factor 2);
 4. whole-body transverse echo planar imaging (EPI) DWI (TR 10 500 ms, TE 78 ms, diffusion weightings (b-values): 0, 500 and 1000 s/mm², matrix size 160, 5 mm slices, 40 slices, FoV 450 mm, GRAPPA, acceleration factor 2; 2 averages);
 5. a transverse T1-weighted fast low angle shot (FLASH) gradient echo sequence (TR 1510 ms, TE 2.15 ms, inversion time (TI) 1200 ms, matrix size 320, 5 mm slices, FoV 400 mm, GRAPPA, acceleration factor 2);
 6. a coronal half Fourier acquisition single shot turbo spin echo sequence (HASTE) of the thorax (TR 649 ms, TE 51 ms, matrix size 320, 6 mm slices, FoV 330 mm, GRAPPA, acceleration factor 2);
 7. a coronal 3-dimensional VIBE sequence of the thorax (TR 3.66 ms, TE 1.29 ms, matrix size 192, 4 mm slice thickness, FoV 350 mm, GRAPPA, acceleration factor 2)
 8. a coronal 3-dimensional VIBE sequence of the thorax after i. v. administration of gadolinium with a delay of 2 min (TR 3.67 ms, TE 1.29 ms, matrix size 192, 4 mm slice thickness, FoV 350 mm, GRAPPA, acceleration factor 2);
 9. a coronal 2 D turbo inversion recovery sequence with magnitude (TIRM) with short TI for fat suppression in free-breathing of the whole body (TR 3190 ms, TE 55 ms, matrix size 384, 5 mm slice thickness, FoV 450 mm, GRAPPA, acceleration factor 2)

PET/MRI image fusion was performed for the post-contrast T1-weighted VIBE images and the T2-weighted blade images.

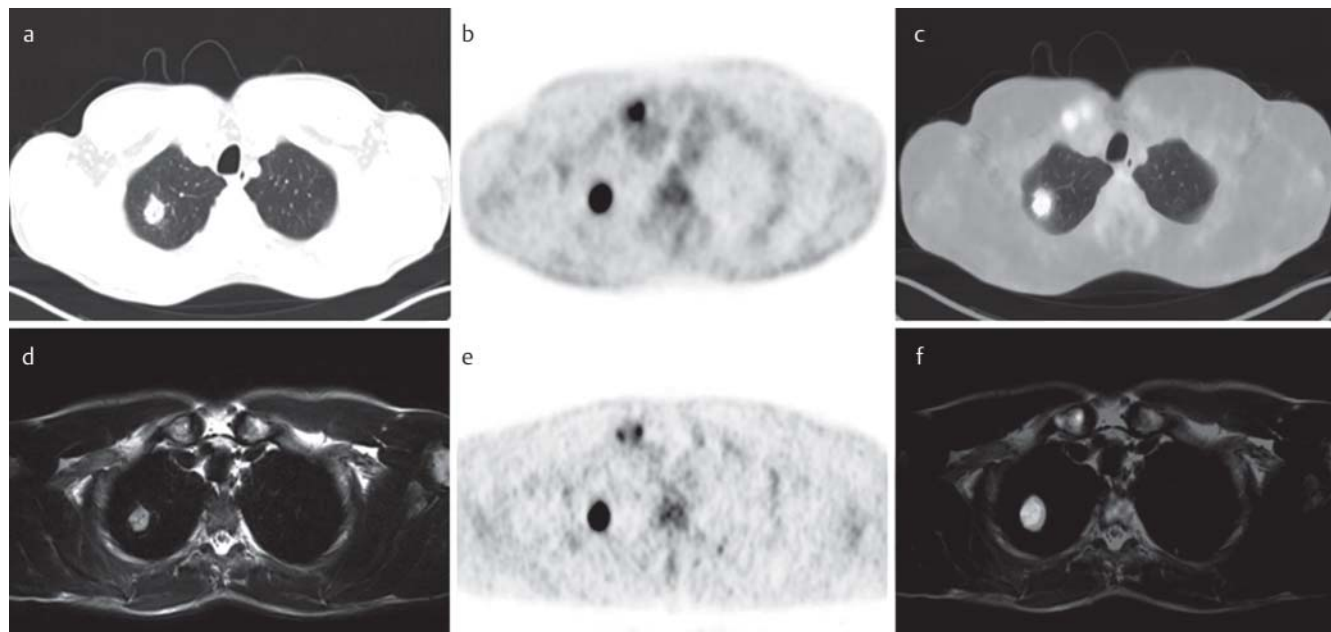


Fig. 1 ¹⁸F-FDG avid, histological proven NSCLC in the right upper lobe of a 44 year-old male patient on CT **a**, on PET after CT-based attenuation correction **b** and on the fused FDG-PET/CT image **c**. Identical tumor mass of the same patient in the right upper lobe on T2w blade MR image **d**, clearly visible on the MR attenuation corrected-PET image, and on FDG-PET/MR **f**.

Image Analysis

Two readers with 8 and 4 years of experience in MRI and 8 and 6 years of experience in hybrid PET/CT imaging analyzed the images in consensus and in random order using a picture archiving and communication system (Centricity; General Electric Medical Systems, Milwaukee, WI, USA) and a dedicated viewing software for hybrid imaging (Syngo.via; Siemens, Healthcare Sector, Erlangen, Germany). Tumor borders of the primary lung cancer were identified on axial slices of the CT scan or T1w images and a polygonal volume of interest (VOI) was placed on fused PET/CT or PET-MR images (► **Fig. 1**), covering the entire tumor manifestation to determine the mean and maximum standardized uptake value (SUV_{max}; SUV_{mean}).

For ADC analysis, DWI data were transferred to an external workstation equipped with the custom software STROKETOOL (<http://www.digitalimagesolutions.de>). ADC parameter maps were computed using the following formula:

$S(b) = S_0 e^{-ADC_{mono} \cdot b}$ with $S(b)$ = signal intensity at b-value b , S_0 = signal acquired without diffusion sensitizing gradients and ADC_{mono} = diffusion coefficient. For further analysis, a polygonal region of interest (ROI) was manually drawn on $b = 0$ images encompassing the entire area of the targeted lesions by one author with 8 years of experience in body MR imaging and then transferred to the corresponding parameter maps (► **Fig. 2**) using the STROKETOOL software.

In order to ensure proper positioning of the ROI on the $b = 0$ images, the contrast-enhanced T1-weighted images were reviewed during the placement of the ROI. ADC_{mean} values were determined for all lung tumors. The mean ADC was defined as the mean value of all tumor pixels in the assessed ADC slices.

Abb. 1 ¹⁸F-FDG aufnehmendes, histologisch gesichertes NSCLC im rechten Lungenoberlappen eines 44-jährigen, männlichen Patienten in der CT-Untersuchung **a**, im PET nach der CT-basierten Schwächungskorrektur **b** und in der fusionierten FDG-PET/CT Untersuchung **c**. Der identische Primarius desselben Patienten im rechten Lungenoberlappen in der T2-gewichteten blade MRT-Sequenz **d**, klar sichtbar in der MRT-basierten, schwächungskorrigierten PET und in der FDG-PET/MRT.

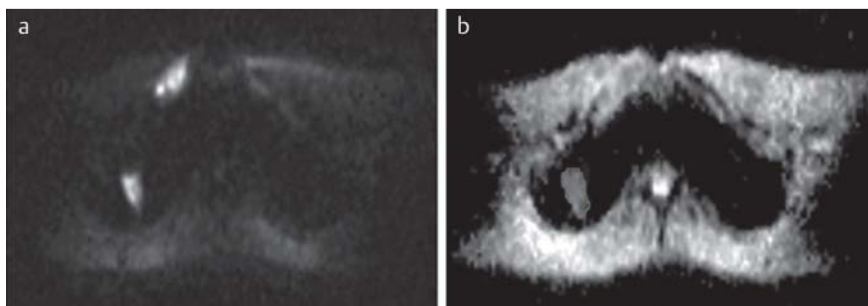


Fig. 2 Increased signal intensity on the b1000 DWI image of a NSCLC located in the right upper lobe **a** and with the tumor appearing as an area of low signal intensity on the corresponding ADC map **b**.

Abb. 2 Gesteigerte Signalintensität eines NSCLC im rechten Oberlappen in der b1000 DWI **a**. Der Tumor erscheint signalabgesenkt in der korrespondierenden ADC Karte **b**.

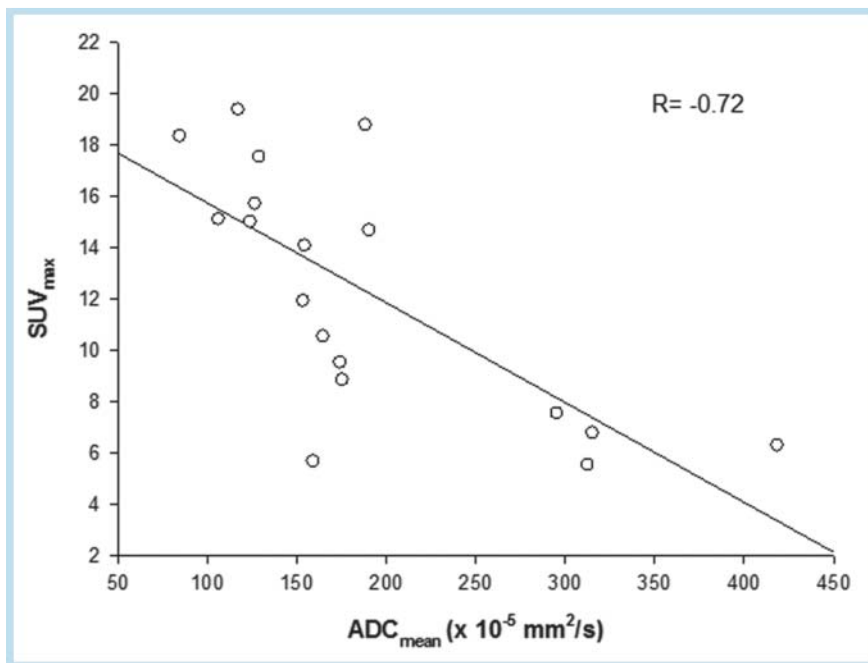


Fig. 3 Scatter plot showing a significant inverse correlation between the ADC_{mean} and the SUV_{max} (R = -0.72; p < 0.001).

Abb. 3 Das Streudiagramm zeigt eine signifikante, inverse Korrelation zwischen dem mittleren ADC und dem SUV_{max} (R = -0.72; p < 0.001).

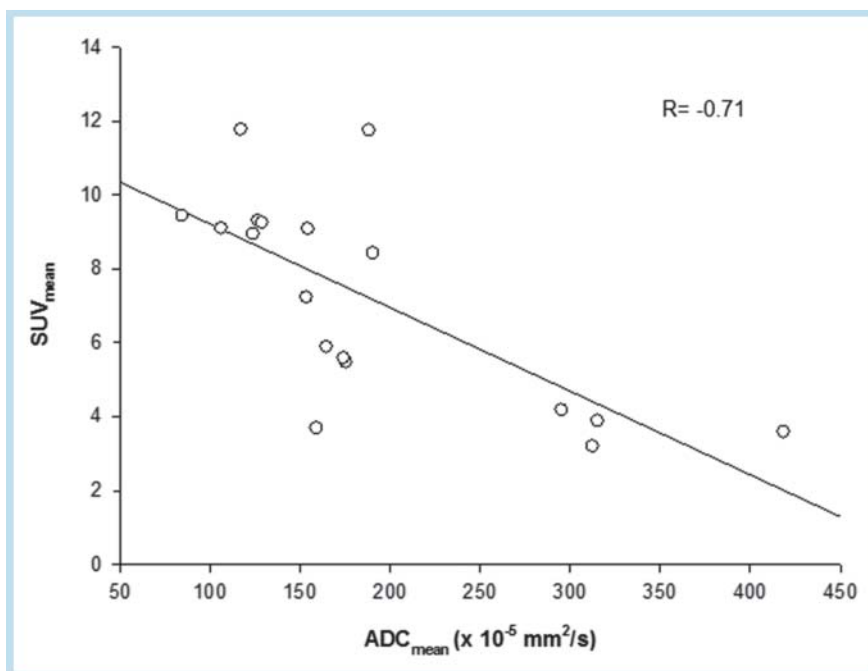


Fig. 4 Scatter plot showing a significant inverse correlation between the ADC_{mean} and the SUV_{mean} (R = -0.71; p < 0.001).

Abb. 4 Das Streudiagramm zeigt eine signifikante, inverse Korrelation zwischen dem mittleren ADC und dem SUV_{mean} (R = -0.71; p < 0.001).

This document was downloaded for personal use only. Unauthorized distribution is strictly prohibited.

Reference Standard

Tumor histopathology was confirmed with percutaneous needle biopsy, endobronchial ultrasound biopsy, or thoracotomy in the 18 patients. Nine patients had adenocarcinomas, seven patients had squamous cell carcinomas, and two patients had large cell carcinomas.

Statistics

Statistical analysis was performed using SPSS 20™ (SPSS Inc., Chicago, IL, USA). Data are presented as means \pm standard deviation (SD). Descriptive analysis was used for SUV_{max} and SUV_{mean} of the tumor tissue. Pearson's correlation coefficients were calculated to compare SUV and ADC values. A p -value ≤ 0.05 was considered to indicate statistical significance.

Results

FDG-PET/CT and FDG-PET/MRI acquisitions were completed successfully in all 18 patients. The mean delay between FDG-PET/CT and FDG-PET/MRI was 80 ± 13 min.

The SUV_{max} of NSCLC was 12.3 ± 4.8 , and the SUV_{mean} was 7.2 ± 2.8 assessed by FDG-PET/MRI. For FDG-PET/CT the SUV_{max} of NSCLC was 12.7 ± 4.6 , and the SUV_{mean} was 7.5 ± 2.7 . The SUV_{max} measurements derived from FDG-PET/CT and from FDG-PET/MRI exhibited an excellent correlation ($R = 0.93$; $p < 0.001$). Also, the SUV_{mean} for FDG-PET/CT and for FDG-PET/MRI had an excellent correlation ($R = 0.92$; $p < 0.001$).

The tumor ADC_{mean} for all patients was $187.9 \pm 88.8 \times 10^{-5} \text{ mm}^2/\text{s}$ and exhibited a significant inverse correlation with the SUV_{max} ($R = -0.72$; $p < 0.001$) (◉ Fig. 3) as well as with the SUV_{mean} assessed by FDG-PET/MRI ($R = -0.71$; $p < 0.001$) (◉ Fig. 4). Furthermore, the ADC_{mean} exhibited a significant inverse correlation with the SUV_{max} ($R = -0.76$; $p < 0.001$) as well as with SUV_{mean} assessed by FDG-PET/CT ($R = -0.77$ $p < 0.001$).

Discussion

For NSCLC a significant correlation between ADC values and SUV values derived from FDG-PET/CT has been reported [18]. Whole-body integrated PET/MRI scanners provide diagnostic image quality and comparably good lesion characterization and tumor staging in pulmonary masses as compared with PET/CT [16]. In this study we were able to demonstrate a significant inverse correlation of the SUV and ADC values assessed with simultaneous PET/MRI examination.

MR imaging combined with PET requires an accurate correction of detected annihilation quanta for the attenuation effect caused by different body tissues. The major difficulty of MRAC lies in the fact that the MR signal is not related to the radiodensity of the examined tissue and therefore cannot directly be used for attenuation correction. A discrepancy in MRAC and CTAC may result in differences in quantitative SUV measurements, potentially leading to a misinterpretation of the PET-MR data. However, SUV measurements were reported to be robust and provide a high reproducibility using ^{18}F -FDG-PET/CT in NSCLC lesions [20]. In oncologic patients examined with PET/CT and PET/MRI, the SUV_{max} and SUV_{mean} values generally correlate well in normal organ tissues [21]. Furthermore, SUV measurements revealed a high correlation between mean SUVs measured with PET/MRI and PET/CT in lesions [15]. Concordantly, there was a significant correla-

tion in this study between the SUV_{max} and SUV_{mean} of the NSCLCs when assessed by a simultaneous PET/MRI and PET/CT for NSCLC patients. Hybrid PET/MRI is often performed following clinically indicated PET/CT, leading to a longer uptake time from tracer injection in PET/MRI scans. This delay potentially causes different absolute organ distribution and physiological washout of ^{18}F -FDG. In the present study we expected higher SUVs in PET/MRI due to tracer accumulation in malignant tissue. Surprisingly we experienced the opposite. One potential explanation is a difference regarding the type of PET attenuation correction. However, our findings are concordant with recently published PET/MRI studies by Drzezga et al. and Wiesmüller et al. [15, 22].

The potential of FDG-PET/CT for staging in patients with diagnosed NSCLC has been demonstrated [2, 23]. Based on SUV changes, ^{18}F -FDG uptake can determine patient prognoses after treatment [24, 25] and predict tumor response [26]. On the other hand, DWI also has an established role in tumor detection [11] and response assessment. Ohno et al. evaluated the prognostic value of the ADC in NSCLC patients undergoing chemoradiotherapy, suggesting that DWI measurements may be superior to FDG-PET/CT in the prediction of tumor response [27]. Image acquisition significantly differs between DWI and PET as DWI yields information on motion of water molecules representing tissue cellularity, whereas PET measurements yield information about tissue metabolism. However, FDG uptake correlates with the number of viable tumor cells, thus high cellularity may also lead to an increase in FDG uptake. This may be the explanation for the relationship between both aspects (DWI and metabolism) reported in previous studies [25]. Our study demonstrated an inverse correlation between FDG uptake and ADC supporting the theory of increasing FDG uptake and decreasing ADC with increasing cellularity.

While in B-cell lymphomas and invasive ductal carcinomas no correlation was found between ADC and SUV values on PET/CT [28, 29], a significant inverse correlation between SUV and ADC values was reported for GIST, rectal cancers and head and neck squamous cell carcinomas [30–32]. This difference may be explained by tumor heterogeneity. For NSCLC, a significant inverse correlation was found between the SUV_{max} and ADC_{min} , whereas no significant correlation was found when comparing the ADC_{mean} vs. the SUV_{mean} or the ADC_{mean} vs. the SUV_{max} [18]. In contrast, we were able to demonstrate a significant inverse correlation between the ADC_{mean} and the SUV_{max} and between the ADC_{mean} and the SUV_{mean} . This discrepancy may be due to the simultaneous coregistration of the PET and MRI datasets in our study, whereas Regier et al. performed PET/CT measurements within 30 days prior to the MR examination [18]. ROIs were drawn manually by a radiologist and might potentially include parts of the surrounding lung tissue. This might lead to a very low ADC_{min} value, if pixels containing healthy lung tissue are erroneously included in the ROI measurement. In contrast, the ADC_{mean} is generally accepted as a more reliable indicator of tumor cellularity and aggressiveness since the entire lesion is taken into account. Hence, we did not examine the ADC_{min} in our study. It has to be taken into account that measured ADC values strongly depend on the exact choice of b -values, different field strengths and diffusion encoding techniques [33]. In the present study we chose a range of three b -values (b_0 - b_{500} - b_{1000}), because the whole-body PET/MRI system is foremost designed for and used in oncologic applications. With our choice of b -values, we met the consensus recommendations on the use of DWI as an image biomarker in cancer patients [34]. Furthermore, as

demonstrated previously in human brains, ADC values can be reliably calculated using only 2 b-values [35]. To the best of our knowledge, the robustness and repeatability of DWI has not been investigated in NSCLC lesions so far. Several factors may affect ADC quantification, for example the choice of b-values, tissue perfusion [36] or scanner geometry and field strengths [37]. Therefore, the ADC values reported for different cancer types might exhibit significant variations. However, looking at the reproducibility of ADC measurements, recent studies in transplanted kidneys and liver metastases of colorectal carcinoma have shown a high reproducibility with a coefficient of variation below 10% [38, 39]. Up to now, it is unclear if this high reproducibility is transferable to DWI of lung cancer. Future studies are required to investigate this issue, as a high robustness is a prerequisite for the use of DWI in treatment monitoring. A recently published study using an ice water phantom has demonstrated that DWI data acquisition using a DWI protocol designed for comparability across scanners might compensate differences in scanner geometry leading to a high robustness of ADC measurements [40]. However, based on our data, studies on the combined use of ADC and SUV values derived from PET/MRI for the prediction of therapy response are rewarded.

This study has some limitations. First, due to the length of the examination, we did not use respiratory gating for DWI measurements. Second, because tumor grading was not available for all patients, we did not test for a potential correlation between tumor grading and the SUV or ADC. Overall, the number of included patients is relatively low. Therefore, these first results need further confirmation.

In conclusion, this simultaneous PET/MRI study corroborates the assumed significant inverse correlation between increased metabolic activity on FDG-PET and restricted diffusion on DWI in NSCLC. The simultaneous acquisition of the ADC and SUV results in complementary information of the assessed cancer tissue. Further studies are required to investigate the correlation of the SUV and ADC with regard to the underlying histology and tumor response after chemotherapy.

Affiliations

- 1 Department of Diagnostic and Interventional Radiology, D-40225 Düsseldorf, Germany, Univ Düsseldorf, Medical Faculty, Düsseldorf
- 2 Department of Medical Oncology, D-45147 Essen, Germany, Univ Duisburg-Essen, Medical Faculty, Essen
- 3 Department of Diagnostic and Interventional Radiology and Neuroradiology, D-45147 Essen, Germany, Univ Duisburg-Essen, Medical Faculty, Essen
- 4 Department of Nuclear Medicine, D-45147 Essen, Germany, Univ Duisburg-Essen, Medical Faculty, Essen

References

- 1 Jemal A, Bray F, Center MM *et al*. Global cancer statistics. *CA: a cancer journal for clinicians* 2011; 61: 69–90
- 2 Antoch G, Stattaus J, Nemat AT *et al*. Non-small cell lung cancer: dual-modality PET/CT in preoperative staging. *Radiology* 2003; 229: 526–533
- 3 Cerfolio RJ, Bryant AS, Ohja B *et al*. The maximum standardized uptake values on positron emission tomography of a non-small cell lung cancer predict stage, recurrence, and survival. *J Thorac Cardiovasc Surg* 2005; 130: 151–159
- 4 Regier M, Kandel S, Kaul MG *et al*. Detection of small pulmonary nodules in high-field MR at 3 T: evaluation of different pulse sequences using porcine lung explants. *Euro Radiol* 2007; 17: 1341–1351
- 5 Heusner TA, Kuemmel S, Koeninger A *et al*. Diagnostic value of diffusion-weighted magnetic resonance imaging (DWI) compared to FDG PET/CT for whole-body breast cancer staging. *Eur J Nucl Med Mol Imaging* 2010; 37: 1077–1086
- 6 Wu LM, Gu HY, Zheng J *et al*. Diagnostic value of whole-body magnetic resonance imaging for bone metastases: a systematic review and meta-analysis. *Journal of magnetic resonance imaging: J Magn Reson Imaging* 2011; 34: 128–135
- 7 Eiber M, Holzappel K, Ganter C *et al*. Whole-body MRI including diffusion-weighted imaging (DWI) for patients with recurring prostate cancer: technical feasibility and assessment of lesion conspicuity in DWI. *J Magn Reson Imaging* 2011; 33: 1160–1170
- 8 Kim JK, Kim KA, Park BW *et al*. Feasibility of diffusion-weighted imaging in the differentiation of metastatic from nonmetastatic lymph nodes: early experience. *J Magn Reson Imaging* 2008; 28: 714–719
- 9 Liu Y, Liu H, Bai X *et al*. Differentiation of metastatic from non-metastatic lymph nodes in patients with uterine cervical cancer using diffusion-weighted imaging. *Gynecol Oncol* 2011; 122: 19–24
- 10 Razek AA. Diffusion magnetic resonance imaging of chest tumors. *Cancer imaging: the official publication of the International Cancer Imaging Society* 2012; 12: 452–463
- 11 Matoba M, Tonami H, Kondou T *et al*. Lung carcinoma: diffusion-weighted mr imaging—preliminary evaluation with apparent diffusion coefficient. *Radiology* 2007; 243: 570–577
- 12 Buchbender C, Heusner TA, Lauenstein TC *et al*. Oncologic PET/MRI, Part 2: Bone Tumors, Soft-Tissue Tumors, Melanoma, and Lymphoma. *J Nucl Med* 2012; 53: 1244.52 6
- 13 Herzog H, Van Den Hoff J. Combined PET/MR systems: an overview and comparison of currently available options. *Q J Nucl Med Mol Imaging* 2012; 56: 247–267
- 14 Antoch G, Bockisch A. Combined PET/MRI: a new dimension in whole-body oncology imaging? *Eur J Nucl Med Mol Imaging* 2009; 36 (Suppl 1): S113–S120
- 15 Drzezga A, Souvatzoglou M, Eiber M *et al*. First Clinical Experience with Integrated Whole-Body PET/MR: Comparison to PET/CT in Patients with Oncologic Diagnoses. *J Nucl Med* 2012; 53: 845–855
- 16 Schwenger NF, Schraml C, Muller M *et al*. Pulmonary Lesion Assessment: Comparison of Whole-Body Hybrid MR/PET and PET/CT Imaging—Pilot Study. *Radiology* 2012; 264: 551–558
- 17 Schwenger NF, Pfannenbergl C, Reischl G *et al*. [Application of MR/PET in oncologic imaging]. *Fortschr Röntgenstr* 2012; 184: 780–787
- 18 Regier M, Derlin T, Schwarz D *et al*. Diffusion weighted MRI and 18F-FDG PET/CT in non-small cell lung cancer (NSCLC): does the apparent diffusion coefficient (ADC) correlate with tracer uptake (SUV)? *Euro J Radiol* 2012; 81: 2913–2918
- 19 Buchbender C, Hartung-Knemeyer V, Heusch P *et al*. Does positron emission tomography data acquisition impact simultaneous diffusion-weighted imaging in a whole-body PET/MRI system? *Eur J Radiol* 2013; 82: 380–4
- 20 Marom EM, Munden RF, Truong MT *et al*. Interobserver and intraobserver variability of standardized uptake value measurements in non-small-cell lung cancer. *J Thorac Imaging* 2006; 21: 205–212
- 21 Heusch P, Buchbender C, Beiderwellen K *et al*. Standardized uptake values for [(18)F] FDG in normal organ tissues: Comparison of whole-body PET/CT and PET/MRI. *Eur J Radiol* 2013; 82: 870–876
- 22 Wiesmüller M, Quick HH, Navalpakkam B *et al*. Comparison of lesion detection and quantitation of tracer uptake between PET from a simultaneously acquiring whole-body PET/MR hybrid scanner and PET from PET/CT. *Eur J Nucl Med Mol Imaging* 2013; 40: 12–21
- 23 Kligerman S, Digumarthy S. Staging of non-small cell lung cancer using integrated PET/CT. *Am J Roentgenol* 2009; 193: 1203–1211
- 24 Higashi K, Ueda Y, Arisaka Y *et al*. 18F-FDG uptake as a biologic prognostic factor for recurrence in patients with surgically resected non-small cell lung cancer. *J Nucl Med* 2002; 43: 39–45
- 25 Weber WA, Petersen V, Schmidt B *et al*. Positron emission tomography in non-small-cell lung cancer: prediction of response to chemotherapy by quantitative assessment of glucose use. *J Clin Oncol* 2003; 21: 2651–2657
- 26 Huang W, Zhou T, Ma L *et al*. Standard uptake value and metabolic tumor volume of (1)(8)F-FDG PET/CT predict short-term outcome early in the course of chemoradiotherapy in advanced non-small cell lung cancer. *Eur J Nucl Med Mol Imaging* 2011; 38: 1628–1635
- 27 Ohno Y, Koyama H, Yoshikawa T *et al*. Diffusion-weighted MRI versus 18F-FDG PET/CT: performance as predictors of tumor treatment response and patient survival in patients with non-small cell lung cancer receiving chemoradiotherapy. *Am J Roentgenol* 2012; 198: 75–82
- 28 Wu X, Korkola P, Pertovaara H *et al*. No correlation between glucose metabolism and apparent diffusion coefficient in diffuse large B-cell

- lymphoma: a PET/CT and DW-MRI study. *Euro J Radiol* 2011; 79: e117–e121
- 29 Choi BB, Kim SH, Kang BJ *et al.* Diffusion-weighted imaging and FDG PET/CT: predicting the prognoses with apparent diffusion coefficient values and maximum standardized uptake values in patients with invasive ductal carcinoma. *World J Surg Oncol* 2012; 10: 126
 - 30 Wong CS, Gong N, Chu YC *et al.* Correlation of measurements from diffusion weighted MR imaging and FDG PET/CT in GIST patients: ADC versus SUV. *Euro J Radiol* 2012; 81: 2122–2126
 - 31 Gu J, Khong PL, Wang S *et al.* Quantitative assessment of diffusion-weighted MR imaging in patients with primary rectal cancer: correlation with FDG-PET/CT. *Mol Imaging Biol* 2011; 13: 1020–1028
 - 32 Nakajo M, Nakajo M, Kajiya Y *et al.* FDG PET/CT and diffusion-weighted imaging of head and neck squamous cell carcinoma: comparison of prognostic significance between primary tumor standardized uptake value and apparent diffusion coefficient. *Clin Nucl Med* 2012; 37: 475–480
 - 33 Dale BM, Braithwaite AC, Boll DT *et al.* Field strength and diffusion encoding technique affect the apparent diffusion coefficient measurements in diffusion-weighted imaging of the abdomen. *Invest Radiol* 2010; 45: 104–108
 - 34 Padhani AR, Liu G, Koh DM *et al.* Diffusion-weighted magnetic resonance imaging as a cancer biomarker: consensus and recommendations. *Neoplasia* 2009; 11: 102–125
 - 35 Kuhnke M, Langner S, Khaw AV *et al.* Diffusionsgewichtete MRT- wie viele Diffusionsfaktoren sind notwendig? *Fortschr Röntgenstr* 2012; 184: 303–310
 - 36 Heusch P, Wittsack HJ, Kröpil P *et al.* Impact of blood flow on diffusion coefficients of the human kidney: a time-resolved ECG-triggered diffusion-tensor imaging (DTI) study at 3T. *J Magn Reson Imaging* 2013; 37: 233–236
 - 37 Rao RK, Riffel P, Meyer M *et al.* Implementation of dual-source RF excitation in 3 T MR-scanners allows for nearly identical ADC values compared to 1.5 T MR scanners in the abdomen. *PloS one* 2012; 7: e32613
 - 38 Heijmen L, Ter VoertEE, Nagtegaal ID *et al.* Diffusion-weighted MR imaging in liver metastases of colorectal cancer: reproducibility and biological validation. *Eur Radiol* 2013; 23: 748–756
 - 39 Thoeny HC, Zumstein D, Simon-Zoula S *et al.* Functional evaluation of transplanted kidneys with diffusion-weighted and BOLD MR imaging: initial experience. *Radiology* 2006; 241: 812–821
 - 40 Malyarenko D, Galbán CJ, Londy FJ *et al.* Multi-system repeatability and reproducibility of apparent diffusion coefficient measurement using an ice-water phantom. *J Magn Reson Imaging* 2013; 37: 1238–1246